High-pressure experimental and computational XANES studies of $(Mg,Fe)(Si,Al)O_3$ perovskite and (Mg,Fe)O ferropericlase as in the Earth's lower mantle

O. Narygina,[1,*] M. Mattesini,[2] I. Kantor,[3] S. Pascarelli,[4] X. Wu,[1] G. Aquilanti,[4] C. McCammon,[1] and L. Dubrovinsky[1]

[1]*Bayerisches Geoinstitut, Universität Bayreuth, Bayreuth D-95440, Germany*

[2]*Departamento de Física de la Tierra, Astronomía y Astrofísica I, Universidad Complutense de Madrid, E-28040 Madrid, Spain*

[3]*CARS, University of Chicago, Illinois 60437, USA*

[4]*European Synchrotron Radiation Facility, 38043 Grenoble, France*

(Received 14 January 2009; published 22 May 2009)

Seven iron-containing oxides and silicates including $(Mg_{0.88},Fe_{0.12})SiO$, $(Mg_{0.86},Fe_{0.14})(Si_{0.98},Al_{0.02})O_3$ perovskites, and $(Mg_{0.80},Fe_{0.20})$ ferropericlase were studied using Fe *K*-edge x-ray absorption near edge spectroscopy under pressure up to 85 GPa at ambient temperature. First-principles calculations of Fe *K*-edges of $(Mg_{0.88},Fe_{0.12})SiO$ perovskite and $(Mg_{0.80},Fe_{0.20})O$ ferropericlase were performed using a spin-dependent method. The amount and quality of the data collected allows performance of a systematic study of the absorption edge features as a function of pressure in these geophysically important systems, providing direct experimental validation for band-structure calculations. The comparison between experiment and theory allows analyzing in detail the effect of Fe valence and spin state modifications on the spectra, allowing to confirm qualitatively the presence of a pressure induced spin pairing transition in (Mg,Fe)O ferropericlase and a high-spin intermediate spin crossover in $(Mg,Fe)(Si,Al)O_3$ perovskite.

DOI: 10.1103/PhysRevB.79.174115 PACS number(s): 61.05.cj, 76.80.+y

I. INTRODUCTION

The Earth's lower mantle is believed to consist predominantly of $(Mg,Fe)(Si,Al)O_3$ perovskite with a smaller amount of (Mg,Fe)O ferropericlase and $CaSiO_3$ perovskite. The influence of iron on the properties of these phases is still not fully understood but it is believed that properties such as elasticity, electrical and thermal conductivities, element partitioning between phases, etc. could be significantly affected by the electronic and structural behaviors of iron in minerals under lower mantle conditions.

A number of studies have been carried out to investigate the spin and oxidation states of iron in $(Mg,Fe)(Si,Al)O_3$ perovskite under high pressures. It is known that in the perovskite structure iron can occur in the ferrous (Fe^{2+}) or ferric (Fe^{3+}) valence state. It is well established that ferrous iron occupies the large distorted 8–12-fold coordinated polyhedron while ferric iron might also occupy the smaller octahedral site.[1,2] Electron energy-loss spectroscopy (EELS) and Mössbauer data suggest that the ferric iron fraction in $(Mg,Fe)(Si,Al)O_3$ perovskite depends on the aluminum content: with increasing aluminum concentration the amount of Fe^{3+} increases almost linearly.[3–5]

Using K_β x-ray emission spectroscopy (XES) Badro *et al.*[6] proposed that iron in $(Mg,Fe)SiO_3$ perovskite undergoes a spin crossover at 70 GPa, with a transition to the low-spin state at 120 GPa. Jackson *et al.*[7] investigated the iron spin state in $(Mg,Fe)SiO_3$ perovskite with different iron contents using nuclear forward scattering (NFS), and inferred a high-spin (HS) to low-spin (LS) transition in Fe^{3+} at 70 GPa, with Fe^{2+} remaining in the high-spin state throughout the studied pressure interval. Combining XES and NFS techniques to study $(Mg,Fe)(Si,Al)O_3$ perovskite, Li *et al.*[8] inferred that Fe undergoes a transition from high-spin to low-spin in the pressure range of 20–100 GPa. From these results it appears that the use of only XES and NFS methods was not able to provide a conclusive answer to the question of the iron spin state in magnesium-bearing silicate perovskite at the megabar pressure range.

X-ray absorption near-edge spectroscopy (XANES) directly probes the empty density of electronic states above the Fermi level around the absorber atom. Fe *K*-edge XANES, along with EELS, conventional and synchrotron Mössbauer spectroscopies (NFS), is one of the more precise experimental techniques to follow electronic and local structures around Fe, and can be relatively easily combined with the diamond-anvil cell (DAC) technique for making *in situ* measurements under high-pressure and temperature conditions. In contrast to Mössbauer spectroscopy, XANES does not require ^{57}Fe enrichment of the sample which simplifies the experimental procedure. While conventional Mössbauer spectroscopy gives information over a large region of the sample, it has recently become possible to obtain high quality XANES with the micron resolution enabling the analysis of individual regions within the DAC.[9] Therefore micro-XANES spectroscopy can be a powerful experimental tool for *in situ* high-pressure and/or high-temperature measurements of the local electronic and crystallographic environments of iron. Consequently Fe *K*-edge micro-XANES can provide information that complements the results of other methods (XRD, conventional Mössbauer, NFS, and XES) for examining the spin and oxidation states of iron under Earth's lower mantle pressures.

Up to now, no systematic study has been performed on the evolution of Fe *K*-edge XANES in these geologically relevant systems up to very high pressures. One of the reasons for this is related to the experimental difficulties in obtaining good quality data at such extreme conditions due to the high absorption of the diamond anvils at low x-ray energy (the Fe *K*-edge is at ~7 keV), and to the strong constraint on spot size and stability that these studies impose. Many of these difficulties have been overcome with the use of third

generation synchrotron sources, coupled to advances in x-ray optics and high-pressure techniques.

In parallel, major advances in *ab initio* codes make it now possible to calculate band structures even in complex systems such as transition-metal oxides, and from these obtain theoretical simulations of the absorption spectra, which include both core-hole and spin-polarization effects.

The aim of this study was therefore to take advantage of these recent experimental and theoretical advances to perform a systematic Fe *K*-edge XANES study of several iron oxides and silicates under pressure in order to establish the strengths and limitations of this technique in complementing information on oxidation and electronic states of iron in these compounds, and to define the abilities of the method to investigate spin transitions, particularly in Fe-bearing silicate perovskites.

The paper is organized as follows. In Sec. II we give experimental details on sample preparation, and on preliminary structural and magnetic characterizations (Sec. II A), as well as on the experimental methods used (Sec. II B). Section III reports the Fe *K*-edge XANES results for all the studied systems, and emphasizes the discussion on two issues: the effect of oxidation state (Sec. III A) and the effect of spin state (Sec. III B) on the absorption spectra. Whereas we discuss the former issue globally for the whole set of samples, the latter issue has been focused only on the ferropericlase (Sec. III B 1) and on the perovskite systems (Sec. III B 2). Finally in Sec. IV we report the main conclusions of this work.

II. EXPERIMENTAL

A. Sample preparation and characterization

Seven samples with different $Fe^{3+}/\Sigma Fe$ ratio were studied by means of XANES spectroscopy: Fe_2O_3 (hematite), Fe_3O_4 (magnetite), FeO (wüstite), (Mg,Fe)O (ferropericlase), $FeTiO_3$ (ilmenite), $(Mg,Fe)SiO_3$, and $(Mg,Fe)(Si,Al)O_3$ (perovskites). All samples are synthetic and enriched with the ^{57}Fe isotope (in order to use the same samples for high-pressure Mössbauer spectroscopy).

Hematite Fe_2O_3 is an iron III oxide with a corundumlike structure, with all iron ions occupying octahedral positions. The sample was a commercially available 99.99% purity Fe_2O_3 powder. X-ray diffraction and Mössbauer spectroscopic measurements at ambient conditions show that no other phases except hematite are present in the sample. $Fe^{3+}/\Sigma Fe$ for this sample is defined to be one.

Magnetite Fe_3O_4 is a mixed-valence oxide with an inverse spinel structure. The tetrahedral position is fully occupied with Fe^{3+} ions while the octahedral position is filled with equal amounts of Fe^{2+} and Fe^{3+} ions. Nominally there are two Fe^{3+} ions for every Fe^{2+} ion in the magnetite structure. However magnetite is known to be a nonstoichiometric compound with a small excess or deficit of cations relative to the Fe_3O_4 formula.[10] A polycrystalline sample of magnetite was synthesized by heating metallic ^{57}Fe in air at 1400 °C for 24 h and quenching it into water. Both x-ray diffraction and Mössbauer spectroscopic measurements at ambient conditions show the presence of a pure magnetite phase. It is difficult to measure accurately the degree of nonstoichiometry in magnetite but, based on the relation between magnetite composition, temperature, and oxygen fugacity,[10] we estimate that in our sample the nonstoichiometry parameter δ in the $Fe_{3(1-\delta)}O_4$ formula is approximately 0.02 (maximum possible value). The corresponding $Fe^{3+}/\Sigma Fe$ ratio in our magnetite sample is therefore 0.72.

Wüstite FeO with a rock-salt type structure is known to be a highly nonstoichiometric compound where x in $Fe_{1-x}O$ can reach a value of 0.12. Fe^{2+} ions occupy the octahedral positions. The crystal chemistry of ferric iron in wüstite is complex, involving predominantly octahedral coordination with some minor amount of tetrahedrally coordinated Fe^{3+}. The degree of nonstoichiometry correlates well with the lattice parameter a of the cubic cell, allowing a straightforward determination of ferric iron content using x-ray diffraction at ambient conditions.[11] The polycrystalline sample of wüstite was synthesized from metallic iron powder in a CO/CO_2 gas-flow furnace at 900 °C and $\log(fO_2)=-16$. The resulting powder sample had a lattice constant a of 4.2959(1) Å, corresponding to $Fe_{0.92}O$.[11] It is not straightforward to determine the Fe^{3+} content of wüstite from the Mössbauer spectrum due to the number of strongly overlapping and closely spaced absorption lines which arise due to complex defect clustering. The $Fe^{3+}/\Sigma Fe$ ratio in our wüstite sample was calculated from its composition to be 0.17.[11]

Al-bearing and Al-free silicate perovskite phases were synthesized in a laser heated DAC at 30–35 GPa and approximately 2500 °C from two orthopyroxene starting materials with compositions $Mg_{0.86}Fe_{0.14}Si_{0.98}Al_{0.02}O_3$ and $Mg_{0.88}Fe_{0.12}SiO_3$ (each 61% enriched in ^{57}Fe) that were described in Ref. 3. Run products were found using x-ray diffraction to consist almost exclusively of $(Mg,Fe)SiO_3$ or $(Mg,Fe)(Si,Al)O_3$ perovskite (in aluminum bearing samples traces of SiO_2 stishovite were detected), and chemical compositions were found using the electron microprobe to be the same as the starting materials within experimental uncertainty. The relative concentration of Fe^{3+} was found by means of Mössbauer spectroscopy to be 0.10 (±0.02) and 0.25 (±0.07) for the $Mg_{0.88}Fe_{0.12}SiO_3$ and $Mg_{0.86}Fe_{0.14}Si_{0.98}Al_{0.02}O_3$ perovskite samples, respectively (Fig. 1).

Ilmenite ($FeTiO_3$) was synthesized from a stoichiometric mixture of Fe_2O_3, TiO_2, and ^{57}Fe heated in an evacuated silica tube at 1200 °C for 24 h. X-ray diffraction and Mössbauer spectroscopy showed no other phase to be present except ilmenite, and Mössbauer data showed the amount of Fe^{3+} to be 0.03 (±0.01) (Fig. 1).

Ferropericlase (Mg,Fe)O is a MgO-FeO solid solution with FeO content less than 50%. We studied a polycrystalline sample with $(Mg_{0.8}Fe_{0.2})O$ composition in this work. The sample was synthesized by mixing stoichiometric amounts of MgO and Fe_2O_3, heating overnight at 1200 °C under reducing conditions ($\log fO_2=-17.4$) using a CO/CO_2 gas-flow furnace and quenching into water. The lattice constant a of ferropericlase was measured to be 4.2389(5) Å. The ferric iron content, measured using Mössbauer spectroscopy over a wide pressure range, was found to be 0.05 (±0.01), and this value was used in the present study (Fig. 1).

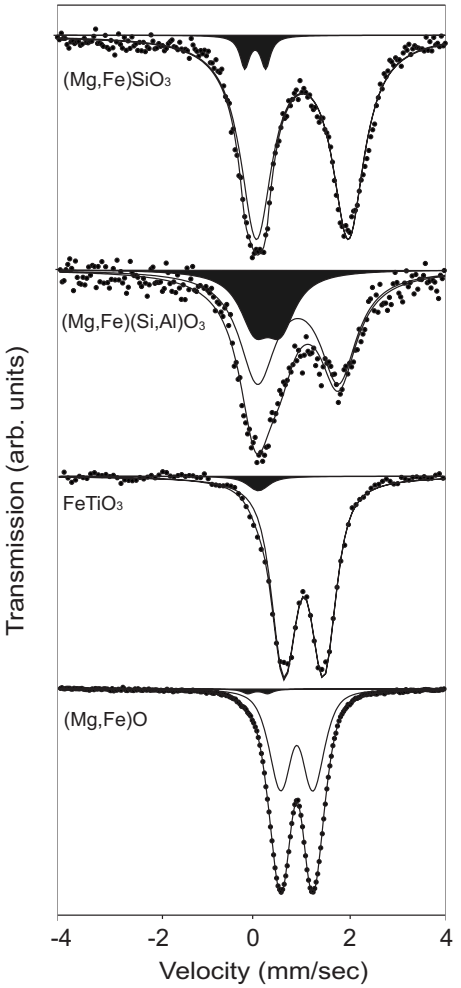

FIG. 1. Mössbauer spectra at ambient conditions of $(Mg,Fe)SiO_3$ and $(Mg,Fe)(Si,Al)O_3$ perovskites, $FeTiO_3$, and (Mg,Fe)O. The spectral area colored in black corresponds to Fe^{3+}.

B. Experimental method

For *in situ* high-pressure micro-XANES and Mössbauer spectroscopy measurements in the DAC, we used diamonds with 250 or 300 μm culet size. Samples were loaded into Re gaskets that had been preintended to ~30 μm and then drilled with a hole of 125 μm in diameter. For pressure calibration and evaluation of the pressure gradient, we used small ruby chips that were loaded into the cell along with the sample. At the highest pressures (~100 GPa) the uncertainty in pressure measurements was estimated to be 5 GPa while the pressure difference between the center and the edge of the pressure chamber was a maximum of 5 GPa. After each increase or decrease in pressure with step ~5 GPa above 30 GPa, samples were annealed at 1700–1900 K by laser heating.

K-edge XANES measurements were performed at the European Synchrotron Radiation Facility at the energy dispersive x-ray absorption spectroscopy (XAS) beamline ID24. The beam was focused horizontally using a curved polychromator Si(111) crystal in Bragg geometry and vertically with a bent Si mirror placed at 2.8 mrad with respect to the direct beam.[12] The Bragg diffraction peaks arising from the diamond anvils were removed from the energy range of interest by changing the orientation of the diamond-anvil cell and following in real time the intensity of the transmitted beam on a two-dimensional detector.

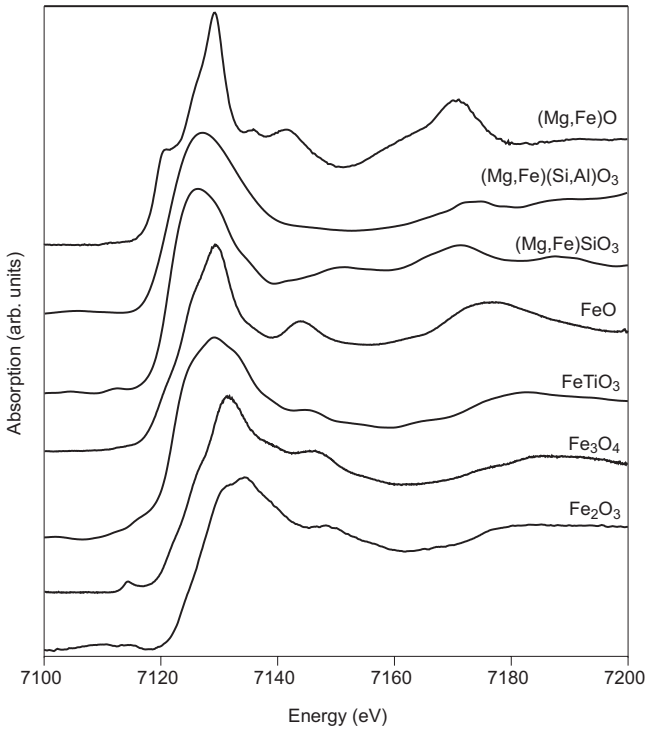

FIG. 2. Normalized XANES spectra taken at 13 GPa from the seven Fe-containing oxides and silicates: (Mg,Fe)O (ferropericlase), $(Mg,Fe)(Si,Al)O_3$ and $(Mg,Fe)SiO_3$ (perovskites), FeO (wüstite), $FeTiO_3$ (ilmenite), Fe_3O_4 (magnetite), and Fe_2O_3 (hematite).

The measured XANES spectra were analyzed using the VIPER program.[13] The flat part of the pre-edge region of the spectrum was fitted to the Victoreen function ($F=a+bE^{-3}$, where E is the absorption energy, and a and b are fit parameters) and this baseline was extended over the entire energy region. The postedge jump in x-ray absorption was then normalized to one.

Transmission Mössbauer spectra were recorded on a constant acceleration Mössbauer spectrometer at temperatures in the range of 300–800 K and pressures in the range from ambient up to above 80 GPa. The experimental procedure is described in detail in McCammon *et al.*[1] and Kantor *et al.*[14]

III. RESULTS AND DISCUSSION

A. Effect of oxidation state

The XANES spectra of all samples at 13 GPa are presented for comparison in Fig. 2. For magnetite (Fe_3O_4), for example, the pre-edge peak structure is well pronounced, which allows extracting information about $Fe^{3+}/\Sigma Fe$ (e.g., in Ref. 15). However in the case of wüstite (FeO), ferropericlase [(Mg,Fe)O], ilmenite ($FeTiO_3$), Al-bearing $[(Mg,Fe)(Si,Al)O_3]$, and Al-free perovskites $[(Mg,Fe)SiO_3]$, the intensity of pre-edge peaks is very weak. In this case the extraction of information about iron oxida-

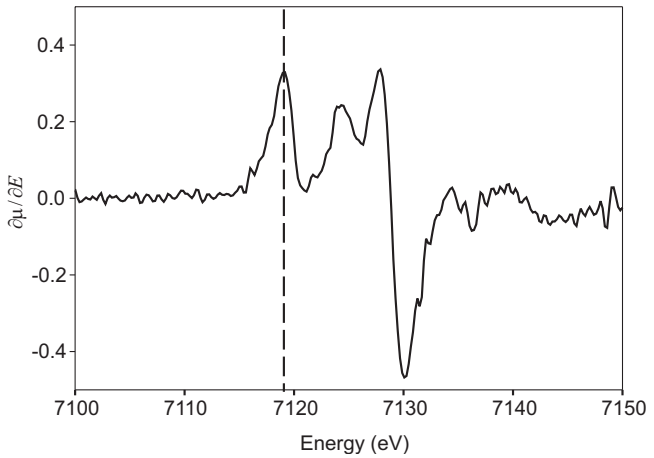

FIG. 3. First derivative of XANES spectrum of (Mg,Fe)O at 1 GPa. The vertical dashed line corresponds to the $1s \rightarrow 4s$ transition peak position that was taken as the absorption edge position.

tion state is challenging, and it is necessary to identify other spectral features that are systematically correlated with the amount of ferric iron. In a previous XANES study of silicate glasses,[15] the following features were proposed: (i) the energy of the main absorption edge, normalized to one at a height of 0.9, and (ii) the areas of the derivative peaks associated with the $1s \rightarrow 4s$ and $1s \rightarrow 4p$ transitions.

For our XANES experimental data the most well defined and reproducible spectral feature is the energy corresponding to the absorption edge, which can be determined from the centroid position of the first peak in the derivative (Fig. 3).

The experimentally obtained edge position energies plotted vs $Fe^{3+}/\Sigma Fe$ at ambient pressure are shown in Fig. 4. For the pure Fe oxides FeO, Fe_2O_3, and Fe_3O_4 a correlation can be made between $Fe^{3+}/\Sigma Fe$ and valence (see dashed line in Fig. 4). On the other hand, the *K*-edge position values for ferropericlase, the perovskites, and for ilmenite are all systematically shifted toward higher energies with respect to the average slope traced by the values of the pure Fe oxides. The addition of Mg or Ti evidently modifies the density of empty states just above the Fermi level with respect to that of the pure Fe oxides, and this strongly affects the shape of the absorption edge. Therefore, whereas the centroid position of the first peak in the derivative is a good fingerprint of Fe valence within the family of pure Fe oxides, it fails when attempting to include Mg and Ti containing Fe oxides.

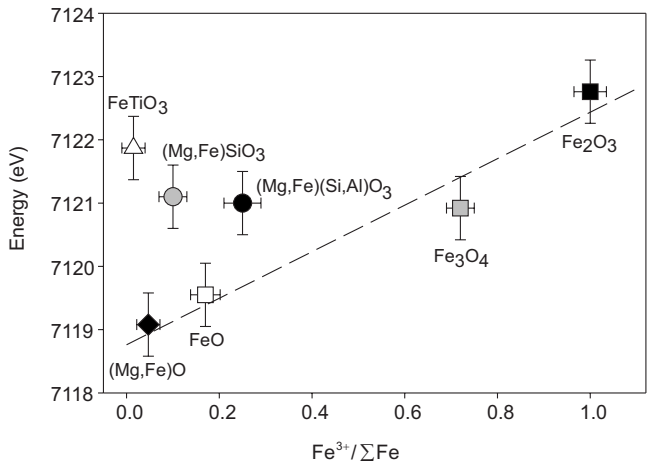

FIG. 4. Absorption edge position energy plotted vs ferric iron content for Fe_2O_3 (black closed rectangle), Fe_3O_4 (gray closed rectangle), FeO (open rectangle), $FeTiO_3$ (open triangle), $(Mg,Fe)SiO_3$ (gray closed circle), $(Mg,Fe)(Si,Al)O_3$ (black closed circle), and (Mg,Fe)O (black closed diamonds). Dashed line represents the fit of the pure oxide data.

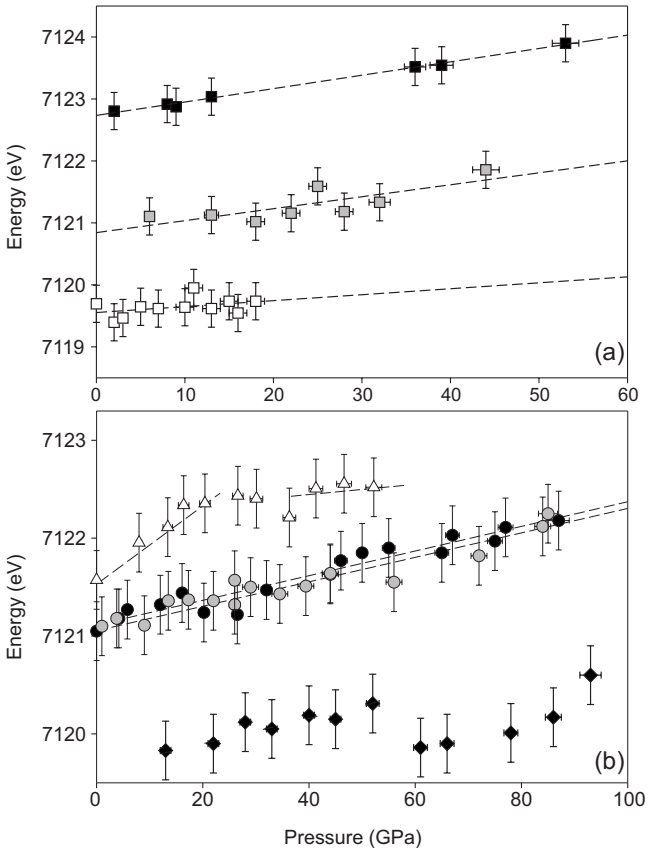

FIG. 5. Evolution of the Fe *K*-edge position with pressure for seven iron oxides and silicates: (a) Fe_2O_3 (black closed rectangles), Fe_3O_4 (gray closed rectangles), and FeO (open rectangles); (b) $FeTiO_3$ (open triangles), $(Mg,Fe)SiO_3$ (gray closed circles), $(Mg,Fe)(Si,Al)O_3$ (black closed circles), and (Mg,Fe)O (black closed diamonds). Dashed lines represent the linear fit of the absorption edge positions.

The effect of pressure on absorption edge position for all studied systems is presented in Fig. 5. Except for $FeTiO_3$ and (Mg,Fe)O the *K*-edge position for studied samples does not show any significant change with pressure apart from a gradual shift toward higher energies (Fig. 5). The pressure evolution of the absorption edge position for $FeTiO_3$ [Fig. 5(b)] shows a peculiarity between 20 and 40 GPa, where the transition to single perovskite phase takes place. This effect is described in detail in Ref. 16. In the case of (Mg,Fe)O [Fig. 5(b)] we observe a discontinuity at ~60 GPa, which perfectly coincides with the previously reported spin transition in ferropericlase.[17,18] We will discuss this point again in the following section.

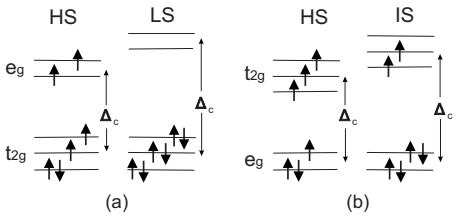

FIG. 6. (a) HS and LS electronic configurations of Fe^{2+} in the octahedral field (ferropericlase case); (b) HS and IS electronic configurations of Fe^{2+} in the distorted cubic field (perovskite case). Δ_C is crystal-field splitting.

B. Effect of spin state

1. (Mg,Fe)O ferropericlase

a. Experimental. The main goal of the study is to examine the ability of XANES to detect spin transitions under high pressure. Therefore $(Mg_{0.80}Fe_{0.20})O$ was chosen as the example system for tracing changes in the absorption of iron through the gradual HS-LS crossover in the compound.

In ferropericlase Fe^{2+} ions occupy octahedral sites; therefore the five $3d$ energy levels are split in three lower $-t_{2g}$ and two higher $-e_g$ energy levels, separated by the crystal-field splitting energy $-\Delta_C$ [Fig. 6(a)].[19] At ambient conditions Δ_C is small compared to the spin pairing energy and therefore the high-spin configuration (two paired and four unpaired electrons) is the most stable one. But with pressure the crystal-field splitting increases and at a certain point [50 GPa for $(Mg_{0.80}Fe_{0.20})O$ ferropericlase[17]] Δ_C becomes higher than the spin pairing energy, making the low-spin configuration energetically favorable. The crossover to the low-spin state modifies not only the electronic field gradient but also the local environment of iron since the Fe-O bond distribution is expected to be modified, and therefore the transition effect on the Fe *K*-absorption edge in (Mg,Fe)O is expected to be significant.

In fact, a close look at the experimental data shown in Fig. 7 highlights clear changes in the shape of the absorption

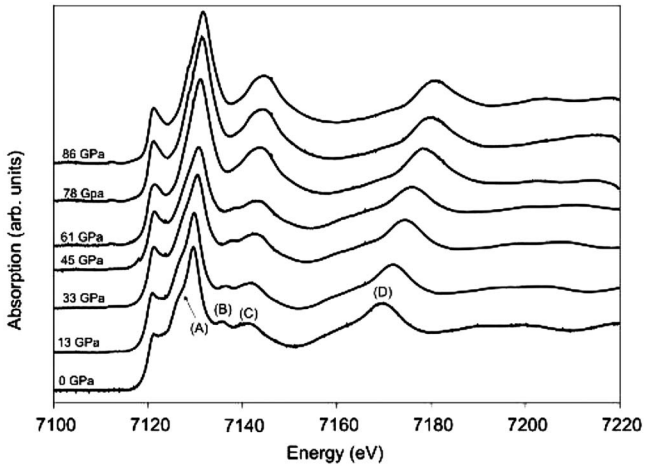

FIG. 7. Experimental XANES spectra of $(Mg_{0.8}Fe_{0.2})O$ ferropericlase as a function of pressure.

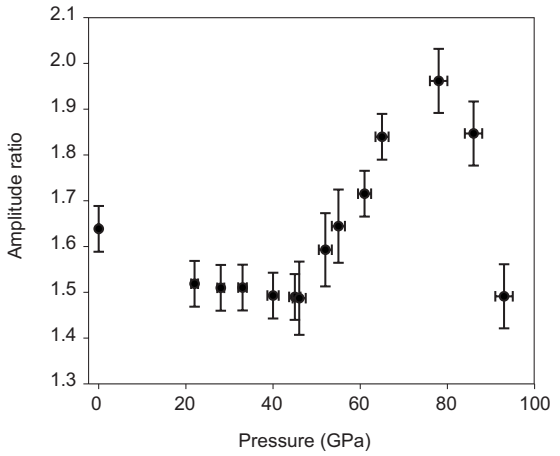

FIG. 8. Pressure evolution of amplitude ratio between the white-line peak at 7130 eV (feature A) and the peak at 7170 eV (feature D) of the $(Mg_{0.80}Fe_{0.20})O$ XANES spectra shown in Fig. 7.

spectra starting from the data at 61 GPa, in addition to the above mentioned anomalous behavior of the absorption edge position: (i) at ambient pressure the main peak in the white-line area is formed by two poorly resolved peaks (feature A) which gradually converge with pressure and finally form one peak of higher intensity; (ii) the small peak at ~7135 eV (feature B) gradually shifts toward high energies and merges with feature C forming an intense single peak ~7140 eV. We note that the changes in the shape of the spectra starting from the data at 61 GPa are rather abrupt. We can help visualize this important change with pressure by plotting the pressure evolution of specific features, such as the amplitude ratio between feature A (the white-line peak, expected to be particularly sensitive to spin state) and feature D, expected to be less sensitive to spin state and more sensitive to local structure. The evolution of this amplitude ratio with pressure obtained from the data of Fig. 7 is shown in Fig. 8. One can clearly see that a significant change occurs between 50–80 GPa, known as the pressure region of the gradual high-spin-low-spin crossover in $(Mg_{0.80}Fe_{0.20})O$ ferropericlase.[17,20] This trend, which highlights the visual changes in the shape of the spectra shown in Fig. 7, can therefore be taken as evidence of the HS-LS transition in this system.

b. Ab initio calculation of x-ray absorption spectra. *Ab initio* calculations were performed for a $2\times2\times2$ MgO supercell (B_1 structure) consisting of a 64-atom cubic system with 29 Mg, 32 O, and 3 Fe atoms.

Theoretical x-ray absorption spectra were computed within the single-particle transition model using the augmented plane-wave (APW) plus local orbital band-structure method,[21] where the exchange and correlation effects were described by means of the generalized gradient approximation.[22] The muffin-tin radii (R_{MT}) for Mg and Si were set to $1.80a_0$; whereas for Fe and O we used $2.0a_0$ and $1.55a_0$, respectively.

Calculations were performed with a plane-wave cutoff corresponding to $R^*_{MT}K_{max}=7$, and by using *s*, *p*, and *d* local

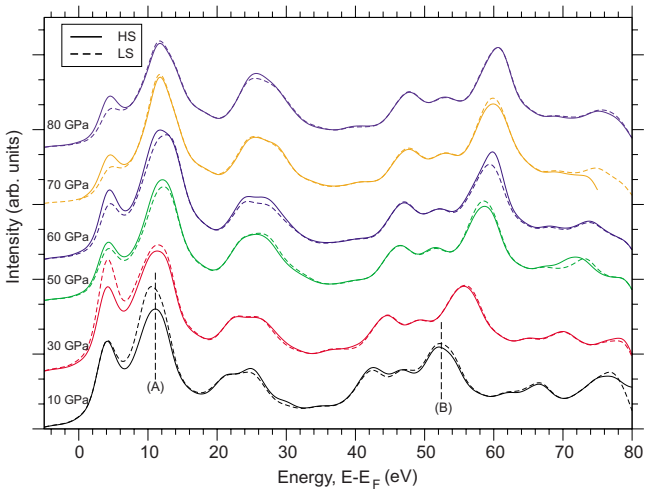

FIG. 9. (Color online) Theoretical Fe *K* edges at different pressures by imposing a fixed spin occupation at the Fe *d* states in the $(Mg_{0.80},Fe_{0.20})O$ ferropericlase system. The onset energy of each spectrum was adjusted according to the variation in the Fermi energy and in the *s* core level energy shift.

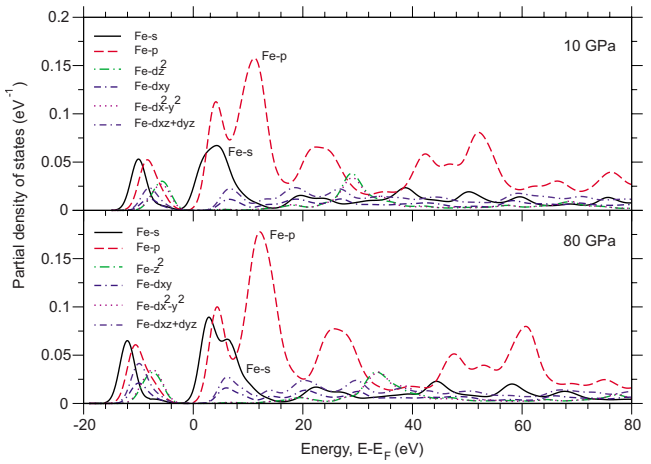

FIG. 10. (Color online) Calculated unoccupied (CB) Fe PDOS for the $(Mg_{0.8},Fe_{0.2})O$ $2\times2\times2$ supercell.

orbitals in the APW basis set to improve the convergence of the wave function. The valence wave functions inside the nonoverlapping muffin-tin spheres were expanded into spherical harmonics up to $l=10$ and the potential up to $l=4$.

The total energy was converged with respect to a $4\times4\times5$ *k*-point sampling corresponding to 24 inequivalent *k* points. Theoretical XAS data were then evaluated at the converged ground-state density by multiplying the angular-momentum projected density of states (DOS) by the transition-matrix elements[23] and accounting for the electric-dipole approximation (i.e., $l\rightarrow l\pm1$ transitions). A direct comparison of the calculated spectra with the measured data was finally achieved by including the instrumental broadening in the form of Gaussian functions corresponding to the experimental resolution of 1.1 eV.

The theoretical Fe *K* edges obtained for a frozen Fe 3*d* shell at different pressure values for both HS and LS configurations are shown in Fig. 9. The 3*d* shell freezing was achieved by selecting a high value for the linearization energy of the Fe 3*d*-atomic orbitals. The vanishing occupied *d* DOS at the absorber Fe site is then reintroduced in the calculation by manually fixing the occupation of the core states. Particularly, we moved the Fe 3*d*,[6] either with a HS or LS configuration, inside the core states and shifted the potential by an appropriate constant. A value of 2.0 was found to be sufficient enough to maintain the entire set of eigenvalues at negative values during the iterative self-consistent-field (SCF) procedure. When the desired energy convergence criterion is reached ($\Delta E\leq0.0001$ Ry), we save the corresponding potential. The final Fe *K* edges were then obtained in a second unfrozen non-SCF calculation, which allow the recovering of the Fe *d* DOS at the frozen site. This procedure was applied for unit-cell volumes corresponding to a pressure range of 0–80 GPa and by imposing a *s* core hole for a divalent Fe configuration. The simulated spectra are able to reproduce the main features of the experimental spectra shown in Fig. 7, underlying the strength of modern *ab initio* codes in modeling complex systems such as these.

From Fig. 9 we see that, for each pressure, the theoretical comparison of the HS and LS calculations shows that the spin state mostly affects the amplitude of the spectral features close to the absorption edge, such as the pre-edge and the white-line amplitude (feature A). This is reasonable and reflects the higher sensitivity of the probed *p* states, through hybridization effects, to the spin-polarized *d* states close to the Fermi level.

In order to confirm this, we have calculated unoccupied conduction-band (CB) Fe partial density of states (PDOS) (Fig. 10) and the occupied [valence-band (VB)] partial Fe, O_1, and O_2 PDOSs for $(Mg_{0.88},Fe_{0.12})O$ ferropericlase (Fig. 11). These figures help in identifying which features of the absorption spectra are more sensitive to local structural modifications, such as bond compression, and which features

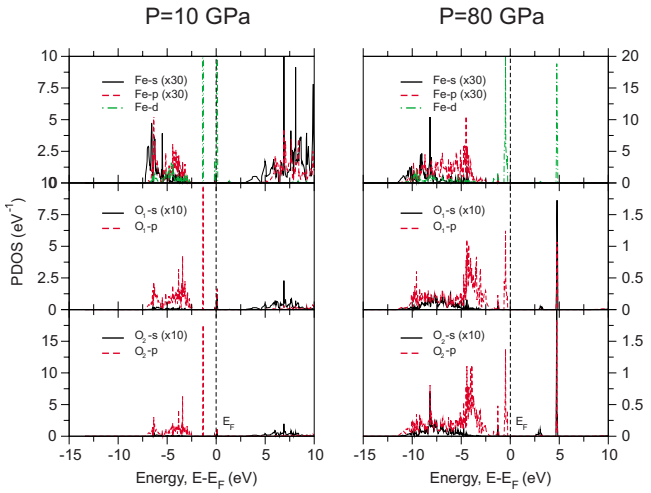

FIG. 11. (Color online) Calculated occupied (VB) partial Fe, O_1, and O_2 PDOS for $(Mg_{0.8},Fe_{0.2})O$ ferropericlase. Note that the atom types O_1 and O_2 constitute the first coordination shell of the absorbing Fe atom.

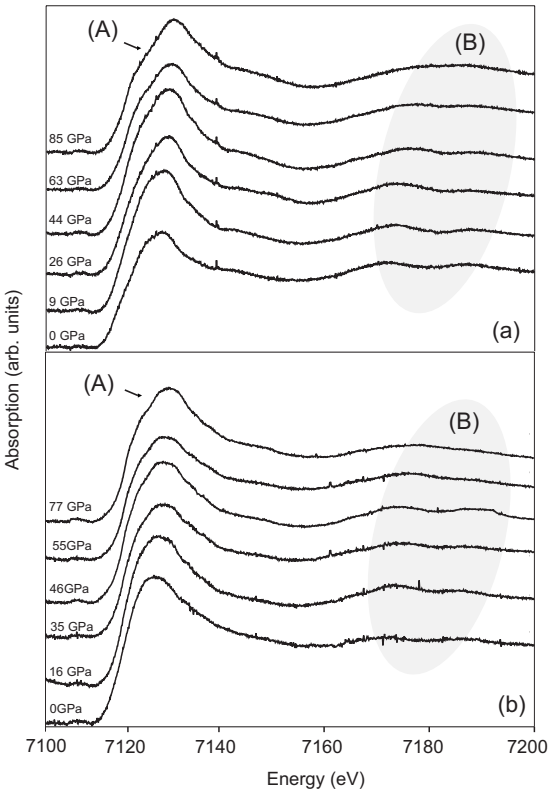

FIG. 12. XANES spectra of (a) $(Mg,Fe)SiO_3$ and (b) $(Mg,Fe)(Si,Al)O_3$ perovskites as a function of pressure.

are more sensitive to spin state.

Figure 10 shows that the spectroscopic signatures mentioned above originate mainly from the high-pressure behavior of the Fe *p* states, which represent the dominant contribution to the spectra at large values of photoelectron energy (i.e., away from the absorption edge region). Figure 11 shows that the oxygen *s* and *p* orbitals hybridize well with the *s*, *p*, and *d* states of Fe, indicating that the spectral shapes shown in Fig. 7 are largely modulated by Fe-O electronic hybridization. The computed bandwidths for Fe and O states become larger, and the electronic density of states get broader as pressure changes from 0 to 80 GPa.

Modifications in spin state are expected to affect mainly the occupied Fe *d* PDOS. Therefore *K*-edge features, mainly sensitive to the unoccupied Fe *p* PDOS, should not be very sensitive to changes in spin state. Spin state effects are readily observable using K_β, emission spectroscopy, which directly probes the occupied Fe *d* states. However, due to hybridization effects, *K*-edge spectroscopy becomes indirectly sensitive to the Fe *d* PDOS through *p*-*d* hybridization. As shown in Fig. 11, the occupied *d* PDOS is localized around the Fermi level. Therefore we expect spin state modifications to affect mainly the region of the spectra close to the absorption edge.

From Fig. 9 we note however that the calculation is not as yet able to reproduce quantitatively the important changes in the shape of the absorption spectra highlighted in Fig. 8. This is most certainly related to the fact that at very low kinetic energies the photoelectron is extremely sensitive to the details of the surrounding potential, setting enormous challenges to the precision of the *ab initio* calculations.

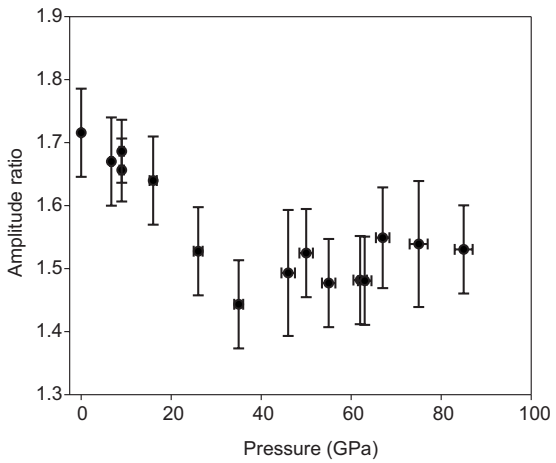

FIG. 13. Pressure evolution of the amplitude ratio between white line at 7130 eV (feature A) and the peak at 7170 eV (feature B) of the XANES spectra of both Al-free and Al-bearing silicate perovskites shown in Fig. 12.

2. $(Mg,Fe)(Si,Al)O_3$ *perovskite*

a. Experimental. Our recent Mössbauer spectroscopic results for both $(Mg,Fe)SiO_3$ and $(Mg,Fe)(Si,Al)O_3$ perovskite phases demonstrate clear changes in the iron electronic state starting at 30–80 GPa.[24] Briefly, at 30 GPa we observe the appearance of a new component with an unusually large quadrupole splitting, close to 4 mm/s, and a central shift about 1 mm/s. We assign this component to an intermediate-spin (IS) state of Fe^{2+}. Thus our Mössbauer spectroscopic results suggest a gradual HS-IS crossover in Fe-bearing magnesium silicate perovskite at 30–80 GPa.

Figure 6(b) illustrates the HS and IS electronic configurations in the perovskite system. Fe^{2+} is located in 8+4-fold coordinated polyhedra, which in a first approximation can be considered as distorted cuboctahedra. The five 3*d* energy levels are split in two lower $-e_g$ and three higher $-t_{2g}$ energy levels which at ambient conditions are populated by two paired and four unpaired electrons—the high-spin configuration. In the intermediate spin configuration four electrons are paired and occupy the lower e_g levels while two unpaired electrons remain on the high t_{2g} energy levels. A crossover to the intermediate spin state increases the value of electric field gradient but does not generate any significant structural change. Therefore the spin crossover effect on the Fe absorption spectra of $(Mg,Fe)(Si,Al)O_3$ perovskite is expected be less pronounced in this system than in the (Mg,Fe)O case.

Absorption spectra of the silicate perovskites, illustrated in Fig. 12, do indicate some changes in the 30–87 GPa range: (i) in the white-line region a small shoulder on the first broad peak appears with increasing pressure (feature A); (ii) in the high-energy region, the two maxima, resolved at low energy, merge forming a broad maximum at 80 GPa (feature B in the highlighted region).

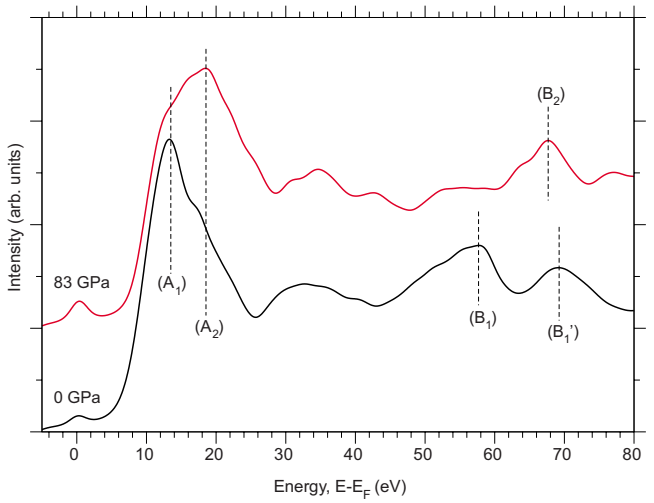

FIG. 14. (Color online) Calculated Fe *K*-edge for $(Mg_{0.88},Fe_{0.12})SiO_3$ perovskite at 0 and 83 GPa. The absorption spectra were computed using the experimental atomic positions and lattice parameters.

As done for the ferropericlase system above, here again we can try to highlight the changes in the shape of the spectra by following the pressure evolution of specific features that have different sensitivities to spin state and local structure. For example, we plot in Fig. 13 the amplitude ratio between the white-line feature (at 7130 eV) and feature B (at 7170 eV), for both Al-free and Al-bearing perovskites as a function of pressure.

This figure shows a weak change in slope at about 35 GPa. We can conclude that Fe *K*-edge absorption spectroscopy can probably detect the spin transition but it has much less sensitivity in perovskites than it does in ferropericlase due to the different mechanism of the transition.

b. Ab initio calculation of x-ray absorption spectra. A similar theoretical spin-dependent method was applied for the $(Mg_{0.88},Fe_{0.12})SiO_3$ perovskite structure as was done for the $(Mg_{0.80}Fe_{0.20})O$ structure. To account for the effect of the Fe s^1 core hole on the electronic band states, the excited iron atom (Fe^{ex}) was formally treated as an impurity inside a perovskite $MgSiO_3$ supercell of dimension $2\times2\times1$ and a background charge was used in order to keep the entire system neutral. The employed model system consists of an 80-atom orthorhombic supercell containing 16 Mg, 48 O, and 16 Si atoms. To achieve the desired 12 wt % Fe concentration one Mg atom was then substituted with Fe.

Figure 14 shows the theoretical Fe *K*-edge spectra calculated at 0 (HS) and 83 GPa (LS) using a self-consistent method to fill the Fe 3*d* states. When applying pressure to $(Mg_{0.88}Fe_{0.12})SiO_3$ perovskite, two main features are seen in the calculated absorption spectra: (i) the onset peak gets broadened and its intensity maximum moves to higher energy values (cf. features A_1 and A_2), and (ii) the two bumps labeled (B_1) and (B_1') convolute into a one single peak (B_2) when going toward high-pressure regimes. Similar changes were registered in the white-line region and in the high-energy part of the measured spectra shown in Fig. 12. This

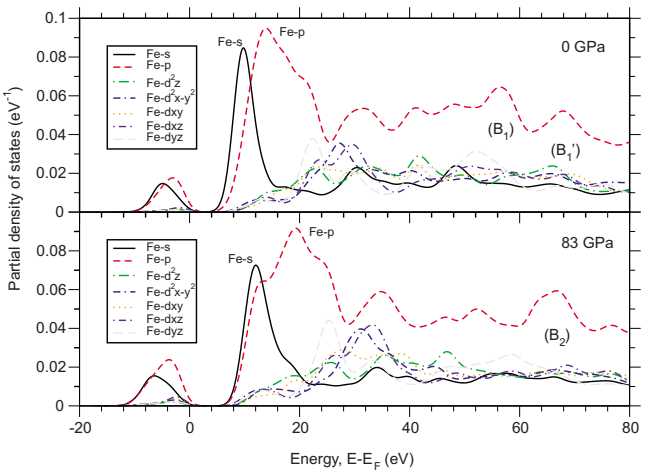

FIG. 15. (Color online) Calculated unoccupied (CB) Fe PDOS for the $(Mg_{0.88},Fe_{0.12})SiO_3$ $2\times2\times1$ supercell. The DOSs were broadened in order to facilitate comparison with the absorption spectra of Fig. 14.

comparison confirms the power of such a calculational scheme in reproducing absorption spectra for band systems that are containing rather delocalized *p* states. Figure 15 represents the calculated unoccupied (CB) Fe PDOS whereas Fig. 16 shows the calculated occupied (VB) partial Fe, O_1, and O_2 PDOS for $(Mg_{0.88},Fe_{0.12})SiO_3$ perovskite.

Figure 15 clearly shows that the spectroscopic signatures mentioned above originate mainly from the high-pressure behavior of the Fe *p* states. The evolution of features (A_1) and (A_2) in Fig. 14 reflect the relative change in the weight of the Fe *s* and Fe *p* PDOS with pressure. Whereas the former undergoes only a slight broadening with compression but does not shift significantly in energy, the latter is strongly affected, with an important broadening and energy shift. Features (B_1), (B_1'), and (B_2) are associated almost uniquely to variations in the Fe *p* PDOS, and are therefore related to the structural variations that occur upon compression of the perov-

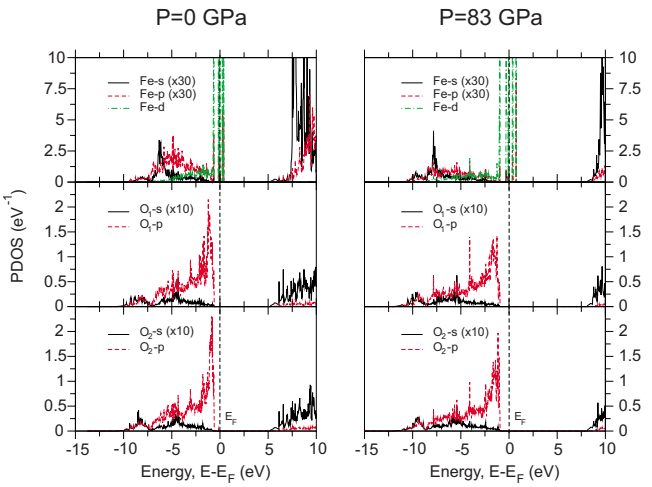

FIG. 16. (Color online) Calculated occupied (VB) partial Fe, O_1, and O_2 PDOS for $(Mg_{0.88},Fe_{0.12})SiO_3$ perovskite. Note that the atom types O_1 and O_2 constitute the first coordination shell of the absorbing Fe atom.

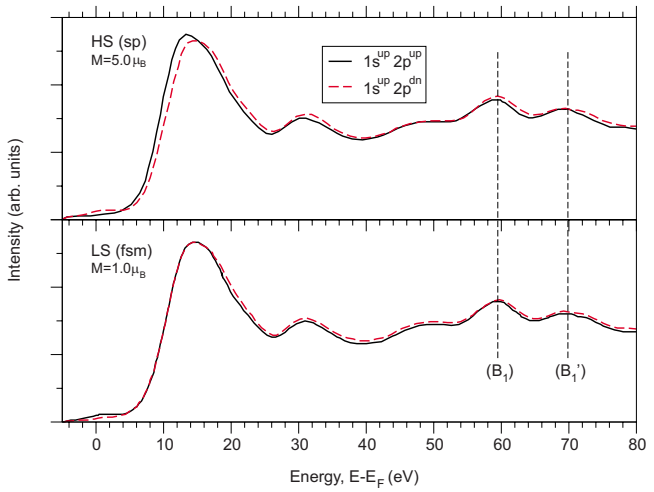

FIG. 17. (Color online) Theoretical Fe K edge at ambient by fixing the Fe d-state occupations in the $(Mg_{0.88},Fe_{0.12})SiO_3$ perovskite model.

skite structure, i.e., to the reduction in the Fe-O distance.

The high-pressure evolution of the Fe K-edge spectra is therefore attributed to the local geometrical modifications that are taking place around the absorbing Fe atom. In particular, when going from 0 to 83 GPa the first coordination shell of iron, which consists of eight-oxygen ions, shrinks considerably, thus enhancing the degree of hybridization between the electronic states that are involved in the Fe-O bonds.

We see from Fig. 16 that the oxygen s and p orbitals hybridize well with the s, p, and d states of Fe, indicating that the spectral shapes shown in Fig. 12 are largely modulated by Fe-O electronic hybridization. As observed for ferropericlase, the computed bandwidths for Fe and O states become larger, and the electronic density of states get broader as pressure changes from 0 to 83 GPa. Here as well, the calculations show that we should expect spin state modifications to affect mainly the region of the spectra close to the absorption edge, where the occupied d PDOS is important.

Spin-polarized s core-hole calculations of the $(Mg_{0.88}Fe_{0.12})SiO_3$ model system were also performed. Using a cell volume corresponding to ambient pressure we first obtained a magnetization of $5.00\mu_B$/cell for a charge-converged spin-dependent calculation, thus describing the low-pressure high-spin (HS) situation. We then performed a fixed spin calculation for the same geometry/volume by imposing a magnetic moment per cell of $1.00\mu_B$ in order to reproduce a low-spin (LS) case. The obtained HS and LS spectra are shown in Fig. 17 with their relative spin-up and spin-down components. It is seen that the high-energy features (B_1 and B_1') are well reproduced in both spin channels for the two different HS and LS cases. Also, spin state is seen to affect (weakly) mainly the energy region close to the absorption edge.

We further ran SCF calculations for a frozen Fe $3d$ shell by using the same theoretical scheme described earlier in Sec. III B 1 b. This procedure was applied for unit-cell volumes corresponding to a pressure range of 0–83 GPa and by imposing a s core hole for a divalent Fe configuration. We confirmed that the high-energy features labeled B_1 and B_1' are also spin-transition independent.

To summarize, for the perovskite system the ambient P theoretical calculations suggest that the effects of a spin transition on the Fe K-edge data are very weak. This is in qualitative agreement with our experimental results discussed above.

IV. CONCLUSION

In this work we take advantage of recent experimental and theoretical improvements to perform a systematic Fe K-edge XANES study on several iron oxides and silicates under very high pressure. The aim is to establish the strengths and limitations of this technique in complementing information on oxidation and electronic state of iron in these compounds, and to define the abilities of the method to investigate spin transitions, particularly in the geophysically important systems: ferropericlase and Al-free and Al-bearing perovskite.

First, we demonstrate that the quality of the data allows providing of direct experimental validation for band-structure calculations. Modern *ab initio* codes are found to be able to simulate the main features of the Fe K-edge XANES spectra in these complex Fe oxides and their evolution with pressure.

Concerning the sensitivity of XANES spectroscopy to the valence state of the absorber, by comparing data on a large variety of samples of known valence at the same pressure, we can conclude that, whereas the centroid position of the first peak in the derivative of the XANES is a good fingerprint of Fe valence within the family of pure Fe oxides, it fails when attempting to include Mg and Ti containing Fe oxides. We attribute this failure to the modifications introduced in the local and electronic structures following the substitution of Fe with other elements. These are reflected in changes in the empty p density of states on Fe, directly probed by Fe K-edge XANES.

In addition, in perovskites, ilmenite, and ferropericlase, it is not possible to extract information on the valence of Fe from the pre-edge feature because this feature is very weak at ambient pressure and remains weak as a function of pressure.

The evolution with pressure of the energy value of the absorption onset is seen to be mainly affected by the effect of bond compression, which makes the edge drift toward higher energy with pressure at a constant rate. Modifications to this behavior are indications of phase transitions, such as observed for ilmenite and ferropericlase.

Concerning the sensitivity of Fe K-edge XANES features to changes in spin state, we conclude that Fe K-edge XANES has variable sensitivity to the spin transition in different systems. In ferropericlase, the HS-LS transition is clearly detected, whereas in the perovskites the effect of the HS-IS transition is visible but less pronounced.

Theoretical calculations are not as yet able to reproduce in a quantitative way the experimental trends observed on the

Fe *K*-edge spectra upon the occurrence of spin transitions but are extremely useful in helping to understand the origin of specific features of the spectra. Moreover, they provide invaluable explanations for the different sensitivity of spectral features to the underlying physics in such complex systems.

ACKNOWLEDGMENTS

We acknowledge the European Synchrotron Radiation Facility for provision of synchrotron time and support. We thank the ID24 beamline technicians Sebastien Pasternak and Florian Perrin for valuable assistance in setting up the experiments. M.M. also wishes to acknowledge the Spanish Ministry of Science and Technology (MCyT) for financial support through the Ramón y Cajal program. The project was financially partly supported by funds from the German Science Foundation (DFG) Priority Program No. SPP1236 under Project No. Mc 3/16-1, and Eurocores EuroMinSci Program.

*Corresponding author; olga.narygina@uni-bayreuth.de

[1] C. A. McCammon, D. C. Rubie, C. R. Ross II, F. Sieifert, and H. St. C. O'Neill, Am. Mineral. **77**, 894 (1992).
[2] C. A. McCammon, Phys. Chem. Miner. **25**, 292 (1998).
[3] S. Lauterbach, C. A. McCammon, P. A. van Aken, F. Langenhorst, and F. Seifert, Contrib. Mineral. Petrol. **138**, 17 (2000).
[4] C. A. McCammon, S. Lauterbach, F. Seufert, F. Langenhorst, and P. A. van Aken, Earth Planet. Sci. Lett. **222**, 435 (2004).
[5] D. J. Frost, C. Liebske, F. Langenhorst, C. A. McCammon, R. G. Trønnes, and D. C. Rubie, Nature (London) **428**(6981), 409 (2004).
[6] J. Badro, J.-P. Rueff, G. Vankó, G. Monaco, G. Fiquet, and F. Guyot, Science **305**, 383 (2004).
[7] J. M. Jackson, W. Sturhahn, G. Shen, J. Zhao, M. Y. Hu, D. Errandonea, J. D. Bass, and Y. Fei, Am. Mineral. **90**, 199 (2005).
[8] J. Li, W. Sturhahn, J. M. Jackson, V. V. Struzhkin, J. F. Lin, J. Zhao, H. K. Mao, and G. Shen, Phys. Chem. Miner. **33**, 575 (2006).
[9] S. Pascarelli, O. Mathon, M. Munoz, T. Mairs, and J. Susini, J. Synchrotron Radiat. **13**, 351 (2006).
[10] R. Aragón, D. J. Buttrey, J. P. Shepherd, and J. M. Honig, Phys. Rev. B **31**, 430 (1985).
[11] C. A. McCammon, and L.-G. Liu, Phys. Chem. Miner. **10**, 106 (1984).
[12] S. Pascarelli, O. Mathon, and G. Aquilanti, J. Alloys Compd. **362**, 33 (2004).
[13] K. V. Klementev, J. Phys. D **34**, 209 (2001).
[14] I. Yu. Kantor, C. A. McCammon, and L. S. Dubrovinsky, J. Alloys Compd. **376**, 5 (2004).
[15] A. J. Berry, H. St. C. O'Neill, K. D. Jayasuriya, S. J. Campbell, and G. J. Foran, Am. Mineral. **88**, 967 (2003).
[16] X. Wu, G. Steinle-Neumann, O. Narygina, I. Yu. Kantor, C. A. McCammon, S. Pascarelli, G. Aquilanti, V. Prakapenka, and L. S. Dubrovinsky, Phys. Rev. B **79**, 094106 (2009).
[17] I. Yu. Kantor, L. S. Dubrovinsky, and C. A. McCammon, Phys. Rev. B **73**, 100101(R) (2006).
[18] J.-F. Lin and T. Tsuchiya, Phys. Earth Planet. Inter. **170**, 248 (2008).
[19] R. G. Burns, *Mineralogical Applications of Crystal Field* (Cambridge University Press, Cambridge, 1970), p. 15.
[20] J.-F. Lin, V. V. Struzhkin, S. Jacobsen, M. Hu, P. Chow, J. Kung, H. Liu, H. Mao, and R. Hemley, Nature (London) **436**, 377 (2005).
[21] P. Blaha, K. Schwarz, G. K. H. Madsen, D. Kvasnicka, and J. Luitz, *WIEN2K, An Augmented Plane Wave Plus Local Orbitals Program for Calculating Crystal Properties* (Vienna University of Technology, Austria, 2001).
[22] J. P. Perdew, K. Burke, and M. Ernzerhof, Phys. Rev. Lett. **77**, 3865 (1996).
[23] J. E. Müller and J. W. Wilkins, Phys. Rev. B **29**, 4331 (1984).
[24] C. A. McCammon, I. Yu. Kantor, O. Narygina, J. Rouquette, U. Ponkratz, I. Sergueev, M. Mezouar, V. Prakapenka, and L. S. Dubrovinsky, Nature Geoscience 1, 684 (2008).